A comparative study on the experimentally derived electron densities of three protease inhibitor model compounds†

Simon Grabowsky,[a] Thomas Pfeuffer,[b] Wolfgang Morgenroth,[c,d,e] Carsten Paulmann,[e,f] Tanja Schirmeister[b] and Peter Luger*[a]

Received 19th February 2008, Accepted 28th March 2008
First published as an Advance Article on the web 2nd May 2008
DOI: 10.1039/b802831a

In order to contribute to a rational design of optimised protease inhibitors which can covalently block the nucleophilic amino acids of the proteases' active sites, we have chosen three model compounds (aziridine **1**, oxirane **2** and acceptor-substituted olefin **3**) for the examination of their electron-density distribution. Therefore, high-resolution low temperature (9, 27 and 100 K) X-ray diffraction experiments on single-crystals were carried out with synchrotron and conventional X-radiation. It could be shown by the analysis of the electron density using mainly Bader's Theory of Atoms in Molecules, Volkov's EPMM method for interaction energies, electrostatic potentials and Gatti's Source Function that aziridine **1** is most suitable for drug design in this field. A regioselective nucleophilic attack at carbon atom C1 could be predicted and even hints about the reaction's stereoselectivity could be obtained. Moreover, the comparison between two data sets of aziridine **1** (conventional X-ray source *vs.* synchrotron radiation) gave an estimate concerning the reproducibility of the quantitative results.

Introduction

The pharmacological action of most drugs is initiated by a recognition process enabling a macromolecular target protein and a low-molecular weight (LMW) ligand to form a complex. Binding of a LMW inhibitor can either be reversible or irreversible. In both cases, the first binding step is the formation of a non-covalent reversible complex, which in case of irreversible inhibitors is followed by a covalent reaction between target and ligand which is not invertible. In each case not only steric interactions but also complementary electronic properties play a dominant role in this recognition process. Whereas steric information can already be provided by the determination of the molecular structure from standard X-ray diffraction experiments using the independent atom model approach, electronic properties can additionally be obtained by high-resolution X-ray diffraction experiments at low temperatures followed by an aspherical electron-density modelling to account for bonding and non-bonding effects.

A molecular association process can be explained by the principle of electrostatic complementarity.[1] This means, steric, electrostatic, van der Waals and hydrogen-bonding interactions will generally cause the molecules to pack in a characteristic way, *i.e.* the molecules will pack in a key–lock arrangement. Therein, regions of charge concentration face electron-deficient regions in adjacent molecules and hydrogen-bond donors will face hydrogen-bond acceptors. These effects of molecular associations are present in a crystalline environment as well as in a protein environment under physiological conditions and can be expected to be comparable in size. As a consequence, quantitative and qualitative properties extracted from the crystallographic experiment provide more information on the intermolecular interactions in a greater assembly than gas-phase computations with isolated molecules. In this study, the tools to describe the reactivity, *i.e.* the rate of the reaction, and the activity, *i.e.* the efficiency of a specific reaction including the selectivity, are derived from the geometry and the electron-density distribution: steric effects, topological electron-density descriptors from a Bader analysis (quantum theory of atoms in molecules[2]), interaction energies from Volkov's exact potential/multipole moment hybrid method (EPMM[3]), electrostatic potentials, zero Laplacian isosurfaces and the source function after Gatti *et al.*[4]

Our aim is to develop cysteine[5] and aspartic[6] protease inhibitors consisting of an electrophilic building block which can covalently block the nucleophilic amino acids of the enzymes' active sites (Cys in cysteine proteases or Asp in aspartate proteases). In the

[a]*Freie Universität Berlin, Institut für Chemie und Biochemie/Kristallographie, Fabeckstr. 36a, 14195, Berlin, Germany*
[b]*Universität Würzburg, Institut für Pharmazie und Lebensmittelchemie, Am Hubland, 97074, Würzburg, Germany*
[c]*Georg-August-Universität, Institut für Anorganische Chemie, Tammannstr. 4, 37077, Göttingen, Germany*
[d]*Aarhus University, Department of Chemistry, Langelandsgade 140, 8000, Aarhus C, Denmark*
[e]*c/o HASYLAB/DESY, Notkestr. 85, 22607, Hamburg, Germany*
[f]*Universität Hamburg, Mineralogisch-Petrologisches Institut, Grindelallee 48, 20146 Hamburg, Germany. E-mail: luger@chemie.fu-berlin.de; Fax: +49 30 83853464; Tel: +49 30 83853411*

† Electronic supplementary information (ESI) available: Local site symmetries applied in the XD2006 refinement strategy, residual density maps, complete lists of bond distances, angles and torsion angles for all compounds, static deformation density and Laplacian maps of olefin **3**, the Espinosa plot including all hydrogen bonds of the compounds, tables for the densities and Laplacians of bond and ring critical points as well as atomic charges and volumes, tables for the source contributions of every atomic basin to the bonds N1/O7–C1, N1/O7–C2 and C1–C2 and experimental data of the model reactions of these compounds with S-, N- and O-nucleophiles. CCDC reference numbers 628198 and 675059–675061. For crystallographic data in CIF or other electronic format and ESI see DOI: 10.1039/b802831a

course of designing optimised inhibitors and to understand the differences in inhibition properties of the scrutinised building blocks we synthesised and crystallised three model compounds **1**, **2** and **3**. These compounds contain the same substituents (two methyl ester groups at C2, *p*-nitrophenyl moiety at C1), but differ in the type of electrophile: aziridine **1**,[7,8] oxirane **2**,[9] or acceptor-substituted olefin **3**[8,10] as shown in Fig. 1.

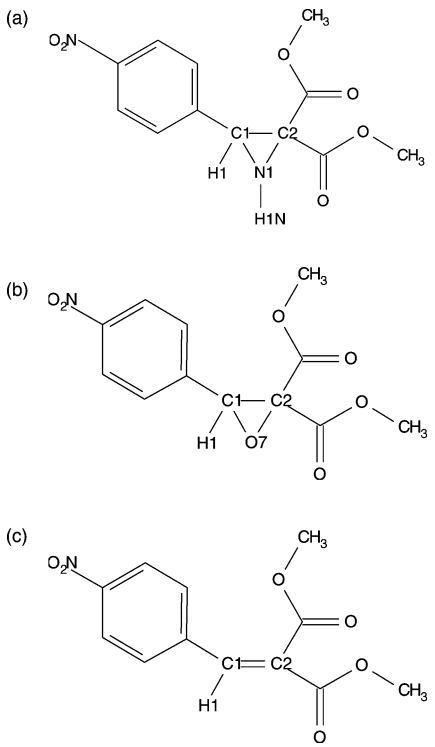

Fig. 1 Molecular structures with atom numbering scheme in the reactive region of (a) aziridine **1**, (b) oxirane **2** and (c) olefin **3**.

At first glance one should expect the oxirane species to be the most reactive compound and the olefin species the least reactive regarding a nucleophilic attack. Moreover, carbon atom C1 should be the preferred centre of attack, because this position is a benzylic one. But as the C–C bond and not the C–X bond is cleaved in these special cases and biological conditions are assumed, the electron-density study grants essential insights into the nature of the reactions. The results obtained from the electron densities will be compared with model reactions of the inhibition process of the three compounds with different model nucleophiles.

The electron-density distributions were derived from high-resolution X-ray diffraction experiments at low temperatures (9, 27 and 100 K) at the synchrotron beamlines D3 and Fl of HASYLAB/DESY and at a conventional Mo-K_α source. The measurements of ultra highly resolved data sets at synchrotron beamlines can be carried out within a few hours so that, together with the use of more and more effective computer hardware and software, the expenditure of time reduces drastically.[11] This enables the screening of electron densities of pharmaceutically promising compounds with acceptable effort. If the nature of the attacking centre of the active site of the protein is known, a screening over functional groups of different ligands that reveal different reactivities can be a very important step in drug design.

Experimental procedures

The three compounds were synthesised as follows: olefin **3** was obtained by Knoevenagel condensation of malonate with *p*-nitrobenzaldehyde. Reaction of **3** with diphenylsulfimide led to aziridine **1** and epoxidation of **3** with hypochlorite yielded oxirane **2**. Compounds **1** to **3** were crystallised from dichloromethane–methanol.

X-Ray synchrotron diffraction experiments of aziridine **1** and olefin **3** were performed at beamline D3 of storage ring DORIS III at HASYLAB/DESY in Hamburg which is equipped with a Huber four circle diffractometer and a marCCD 165 area detector. Wavelengths of 0.560 Å for aziridine **1** and of 0.517 Å for olefin **3** were chosen. The temperature was maintained at 9 K during the measurement by using an open helium gas flow device (Helijet, Oxford Diffraction). In both cases more than 100000 reflections could be measured to a resolution larger than 1.0 $Å^{-1}$ in exposure time periods of about 13 h.

Oxirane **2** was measured at beamline F1 of storage ring DORIS III at HASYLAB/DESY in Hamburg. F1 is equipped with a Kappa-diffractometer and a marCCD 165 area detector. A wavelength of 0.560 Å was adjusted and the temperature was maintained at 100 K using an open flow nitrogen cooling device. About 125000 reflections could be measured to a resolution of 1.2 $Å^{-1}$ within 11 h.

In order to allow a comparison of the synchrotron data with conventional X-ray data, a second measurement of aziridine **1** was performed at the in-house diffractometer. Mo-K_α radiation, a Huber four circle diffractometer and a Bruker APEX CCD area detector were used. The temperature was kept at 27 K in an exposure time period of 10 days with a closed cycle helium cryostat. Although the measurement yielded 50000 less reflections compared to the synchrotron measurement the maximum resolution and the completeness of data were slightly higher. For more details on the measurements and the crystallographic data, see Table 1.

The in-house data set was integrated with the programme SAINT,[12] whereas the synchrotron data sets were integrated with the programme XDS.[13] A programme for the correction of reflection intensities for incomplete absorption of high energy X-rays in the CCD phosphor (oblique correction) for special CCD detectors at HASYLAB was recently published[14] and could successfully be employed for the three synchrotron data sets. Because of this new correction and the newly developed versions of the integration programme XDS and the programme XD for multipole modelling (XD2006[15]), the already published synchrotron data set of aziridine **1**[16] was processed again in order to make sure that all data sets were analysed in the same way and with the newest analysing tools available. For scaling and merging of all four data sets the programme SORTAV[17] was used.

The phase problem was solved with the programme SHELXS[18] and yielded all non-hydrogen atom positions of the asymmetric unit that consists of two molecules for aziridine **1** and one molecule each for oxirane **2** and olefin **3**. Conventional spherical refinement was carried out by the programme SHELXL[18] to establish the starting positional and displacement parameters (anisotropic for non-hydrogen atoms, isotropic for hydrogen atoms) for the aspherical refinement steps. For aspherical refinement the Hansen–Coppens multipole formalism[19] as implemented in the programme XD2006[15] was used. For all four data sets the

Table 1 Experimental details for X-ray diffraction experiments

	Aziridine **1** sync	Aziridine **1** Mo-K_α	Oxirane **2** sync	Olefin **3** sync
Chemical formula	$C_{12}H_{12}O_6N_2$	$C_{12}H_{12}O_6N_2$	$C_{12}H_{11}O_7N_1$	$C_{12}H_{11}O_6N_1$
M/g mol^{-1}	280.24	280.24	281.22	265.22
Space group	$P\bar{1}$	$P\bar{1}$	$P\bar{1}$	$P\bar{1}$
Z	4	4	2	2
a/Å	8.013(2)	8.027(1)	7.746(1)	7.769(2)
b/Å	13.312(3)	13.333(1)	8.080(1)	7.865(1)
c/Å	13.652(2)	13.674(1)	11.835(1)	10.811(1)
α/°	105.98(1)	105.97(1)	86.20(1)	87.61(2)
β/°	106.14(2)	106.05(1)	74.11(1)	85.41(4)
γ/°	107.14(1)	107.14(1)	60.67(1)	62.43(2)
V/Å^3	1231.36	1238.46	619.07	583.67
ρ_x/g cm^{-3}	1.512	1.503	1.509	1.509
F(000)	584.0	584.0	292.0	276.0
μ/mm^{-1}	0.07	0.07	0.08	0.07
Crystal size/mm^3	0.45 × 0.25 × 0.15	0.60 × 0.40 × 0.25	0.60 × 0.40 × 0.15	0.50 × 0.20 × 0.20
Colour	Red	Red	Colourless	Colourless
Beamline	D3	In-house	F1	D3
T/K	9	27	100	9
Wavelength/Å	0.560	0.711	0.560	0.517
sin θ_{max}/λ/Å^{-1}	1.02	1.11	1.19	1.02
No. of collected reflections	163095	113442	126224	104810
No. of unique reflections	18527	23550	14724	9203
No. of reflections with $I \geq 3\sigma$	13753	16994	8523	7557
Completeness (%)	84.5	85.2	84.2	90.2
R_{int} (%)	5.36	4.79	7.62	3.76
Spherical refinement:				
$R(F)$ (%)	4.28	4.66	4.45	4.00
w$R(F^2)$ (%)	11.91	12.51	13.94	12.92
GooF	1.04	1.02	0.97	1.11
Multipole refinement:				
Ratio reflections/parameters	22.81	28.18	20.94	20.26
$R(F)$ (%)	2.92	3.30	3.18	2.67
w$R(F)$ (%)	3.18	3.91	4.38	3.32
GooF	1.03	1.43	0.99	1.47

same chemically most reasonable density model including local symmetries and chemical constraints was applied as far as possible (see also Supplementary Material†). For aziridine **1** the multipole model of the second molecule of the asymmetric unit was completely constrained to that of the first one. Therefore, all electronic results from the multipole modelling presented herein will always refer to an average over both independent molecules. C–H and N–H distances were fixed to average values obtained from neutron diffraction analyses.[20] All non-hydrogen atoms were treated up to the hexadecapole level of expansion, while bond-directed dipoles and quadrupoles were introduced for all hydrogen atoms. The expansion–contraction parameter κ was refined independently for all non-constrained atoms in the three synchrotron data sets, but were fixed to theoretical values calculated by the programme InvariomTool[21] within Dittrich's Invariom approach[22] for the Mo-K_α data set of aziridine **1**. The figures of merit for the data reduction and refinements are collected in Table 1. For analysing the obtained electron-density distributions the programme XDPROP of the XD2006 programme package[15] was used.

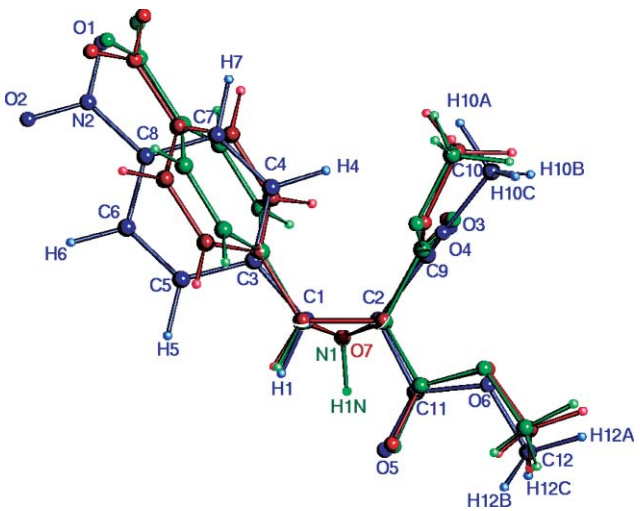

Fig. 2 SCHAKAL[23] superposition of the experimental geometries of aziridine **1** (green), oxirane **2** (red) and olefin **3** (blue). Atom numbering scheme given for olefin **3** coincides with aziridine **1** and oxirane **2**, only additional atoms numbered separately.

Results and discussion

Geometric results

Fig. 2 shows the experimental geometries of the three different molecules aziridine **1**, oxirane **2** and olefin **3**, superimposed in the plane of the three-membered ring, including the atom numbering scheme. The molecular conformations are very similar for aziridine **1** (both molecules, see below) and oxirane **2**, but differ for olefin **3** due to the double bond between C1 and C2. However, in all three cases it is obvious that a nucleophilic attack should occur at carbon atom Cl for steric reasons because the flat aryl ring and

Table 2 Bond distances (Å), angles (°) and torsion angles (°) in the reactive regions of **1**, **2** and **3**; for aziridine **1** averages over the two independent molecules of the asymmetric unit are given

Bond or angle	Aziridine **1** sync	Aziridine **1** Mo-K_α	Oxirane **2**	Olefin **3**
N1/O7–C1	1.4572(6)	1.4603(7)	1.4356(8)	—
N1/O7–C2	1.4596(6)	1.4611(7)	1.4211(7)	—
C1–C2	1.5079(6)	1.5102(7)	1.4877(6)	1.3454(5)
C1–C3	1.4914(6)	1.4935(7)	1.4872(6)	1.4604(5)
C2–C9	1.5078(5)	1.5124(6)	1.5142(6)	1.4955(5)
C2–C11	1.5034(6)	1.5044(7)	1.5161(5)	1.4883(5)
C1–N1/O7–C2	62.26(3)	62.26(3)	62.77(4)	—
N1/O7–C1–C2	58.95(3)	58.90(3)	58.14(3)	—
N1/O7–C2–C1	58.80(3)	58.85(3)	59.09(4)	—
N1/O7–C1–C3	116.48(3)	116.45(4)	117.39(5)	—
C2–C1–C3	119.89(3)	119.89(4)	121.91(4)	130.89(3)
N1/O7–C2–C9	117.16(3)	117.06(4)	116.24(4)	—
N1/O7–C2–C11	115.79(3)	115.88(4)	113.75(3)	—
C1–C2–C9	117.82(3)	117.79(4)	119.00(3)	126.34(3)
C1–C2–C11	116.36(3)	116.43(4)	117.48(4)	117.18(3)
N1/O7–C1–C3–C4	12.6(1)	12.7(1)	−14.7(1)	—
C2–C1–C3–C4	80.4(1)	80.3(1)	53.1(1)	12.8(1)
C1–C2–C9–O4	73.6(1)	73.6(1)	80.0(1)	90.2(1)
N1/O7–C2–C9–O4	140.8(1)	140.8(1)	147.6(1)	—
C1–C2–C11–O6	−145.7(1)	−145.7(1)	−157.0(1)	−176.0(1)
N1/O7–C2–C11–O6	148.1(1)	148.0(1)	136.8(1)	—

the hydrogen atom H1 cause less steric hindrance than the two methoxycarbonyl substituents at C2.

Table 2 shows geometrical properties of the four data sets in the reactive region around the three-membered ring or double bond. For aziridine **1** in both cases an average over the two molecules of the asymmetric unit is shown because the average difference of bond lengths/angles/torsion angles is 0.0015 Å/1.29°/4.1° for the Mo-K_α data set and 0.0017 Å/1.13°/4.1° for the synchrotron data set (*cf.* Supplementary Material†). The agreement of the geometrical data between the two different data sets of aziridine **1** (0.0011 Å for bond lengths, 0.38° for bond angles and 0.5° for torsion angles) shows that one can consider these two geometries as nearly identical although coming from two different measurements.

For the three-membered rings, the C1–C2 bond is longer than found in other aziridines (1.480 Å from ref. 20; 1.460 Å for free aziridine at 145 K as discussed in ref. 16) or oxiranes (1.466 Å from ref. 20; 1.438 Å for free oxirane at 150 K from ref. 24), whereas the C–X bond lengths are shorter or comparable to typical C–X bonds in aziridine (1.472 Å from ref. 20; 1.464 Å and 1.463 Å for free aziridine at 145 K as discussed in ref. 16) or oxirane (1.446 Å from ref. 20; 1.426 Å and 1.435 Å for free oxirane at 150 K from ref. 24). Therefore a widening of the triangle at the hetero atom results due to the special substitution pattern. The same influence of the substitution pattern on the geometry in the biologically active region can be seen for olefin **3**: the C1–C2 double bond distance of 1.3454(5) Å is larger than for an isolated double bond but in the range of a conjugated system like hexatriene (1.345 Å from ref. 20).

Topological analyses

Fig. 3 shows the static deformation density and Laplacian maps of the three-membered rings. The typical banana bond character of all bonds in the strained system can be seen in all maps. Despite the unsymmetrical substitution pattern, the aziridine ring shows a symmetrical distribution of the deformation and Laplacian density. All bonds are normal covalent bonds, the Laplacian map (Fig. 3c) shows the shared interactions (open shell). The values of the density and the Laplacian at the corresponding bond critical points (see Fig. 4 and Supporting Material†) confirm this finding: at N1–C1 and N1–C2 $\rho(\mathrm{bcp}_{N1-C1}) = 1.83(3)$ e Å^{-3} and $\rho(\mathrm{bcp}_{N1-C2}) = 1.80(3)$ e Å^{-3} are very similar and in the range of normal single bonds. The same holds for the Laplacians ($\nabla^2\rho(\mathrm{bcp}_{N1-C1}) = -8.9(1)$ e Å^{-5} and $\nabla^2\rho(\mathrm{bcp}_{N1-C2}) = -7.6(1)$ e Å^{-5}). In Fig. 3b and 3d the static deformation density and Laplacian distribution of the oxirane ring show an unsymmetrical behaviour. Moreover, the Laplacian map in Fig. 3d shows that the bond O7–C1 is an open shell interaction but the bond O7–C2 contains some closed shell contributions. This finding can again be confirmed by the values of the density and the Laplacian at the bond critical points O7–C1 and O7–C2 ($\rho(\mathrm{bcp}_{O7-C1}) = 1.81(4)$ e Å^{-3} and $\rho(\mathrm{bcp}_{O7-C2}) = 1.75(4)$ e Å^{-3}, $\nabla^2\rho(\mathrm{bcp}_{O7-C1}) = -14.3(2)$ e Å^{-5} and $\nabla^2\rho(\mathrm{bcp}_{O7-C2}) = -8.4(2)$ e Å^{-5}). The bond O7–C1 has the higher value of the density at the bcp and the more negative Laplacian value. So this bond shows a more covalent character than the bond O7–C2. It is not clear if this effect is caused by the unsymmetrical substitution pattern or if it is caused by shortcomings in the multipole formalism for C–O bonds[25] (see also Fig. 4).

Fig. 4 visualises the transferability of bond topological properties for the individual bonds of the three compounds. For ρ(bcp) the general agreement looks very satisfactory for cpds. **1–3** while the differences in the Laplacian are more obvious due to the fact that the Laplacian is more sensitive as a second spatial derivative of the density. For the different types of bonds at C1–C2, the difference between a single bond in cpds. **1** and **2** and a double bond in cpd. **3** is 0.7 e Å^{-3} and −15 e Å^{-5}, respectively. For the three different compounds, the average differences for the density and the Laplacian at the bond critical points of all shared bonds are 0.07 e Å^{-3} and 3.6 e Å^{-5}, respectively. Considering the two

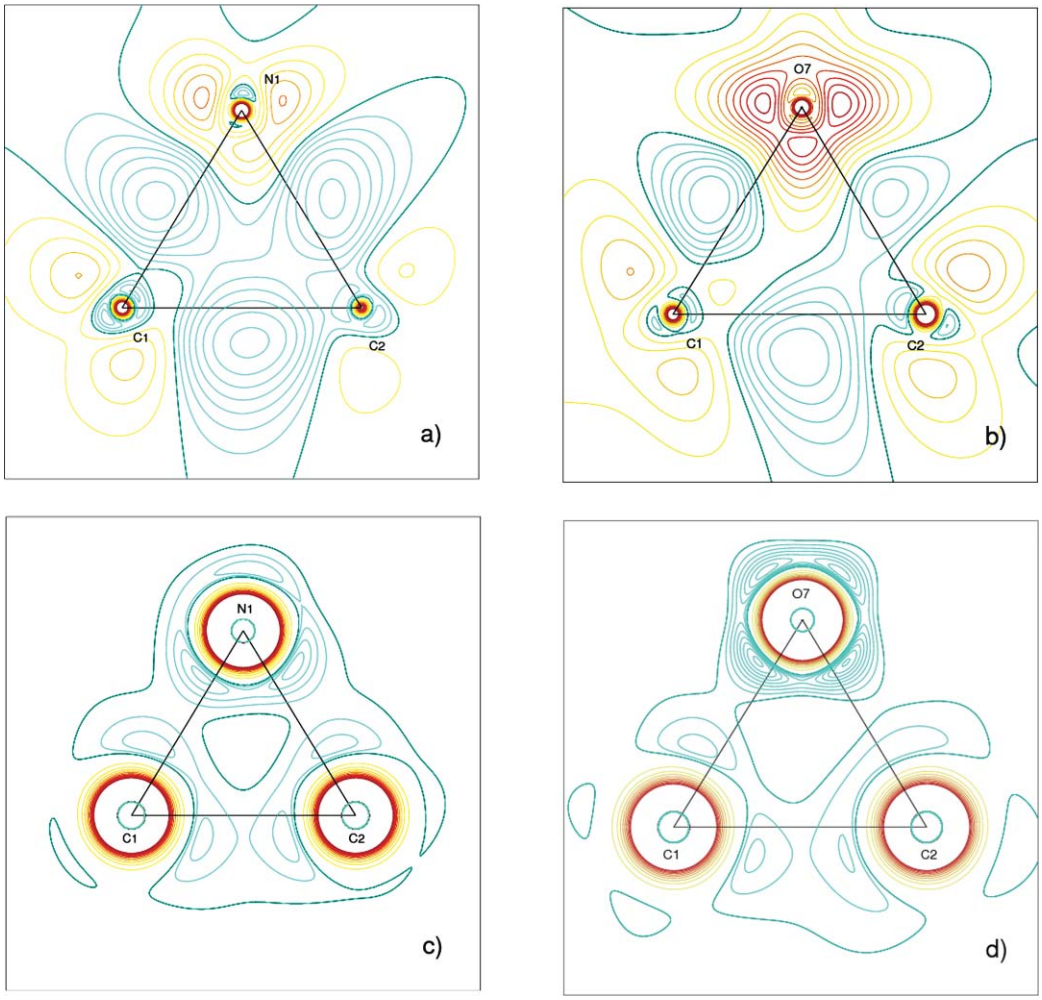

Fig. 3 Static deformation density distribution (blue: positive with contour interval 0.05 e Å^{-3}; red: negative with contour interval 0.1 e Å^{-3}) of a) aziridine ring of **1** (synchrotron data set) and b) oxirane ring of **2**; Laplacian distribution (blue: negative with contour interval 10 e Å^{-5}; red: positive with contour interval 25 e Å^{-5}) of c) aziridine ring of **1** (synchrotron data set) and d) oxirane ring of **2**.

different data sets of aziridine **1**, the average differences for the density and the Laplacian at the bond critical points are 0.06 e Å^{-3} and 4.2 e Å^{-5}, respectively. These agreements are very good and show that reproducibility and transferability are given sufficiently. Average deviations that were found in other studies are 0.07 e Å^{-3} and 4.9 e Å^{-5} for two different modifications of L-alanyl-L-tyrosyl-L-alanine[26] or 0.1 e Å^{-3} and 2 e Å^{-5} for two datasets of a hexapeptide.[27]

Atomic properties

According to Bader's partitioning scheme,[2] atomic properties like charge and volume can be calculated by integrating over the atomic basins. Considering the two data sets of aziridine **1**, the average difference in the charges is 0.13 e and in the volumes 0.38 Å^3. Therefore one can state again, as for the bond properties, that reproducibility between conventional and synchrotron data is fulfilled because the differences are in the range of the typical accuracy in experimental charge density studies (*e.g.* ref. 26). The atomic charges and volumes for the individual atoms are represented in Fig. 5 and 6, respectively.

Transferability is given (average differences for the charges and the volumes of all shared atoms are 0.06 e and 0.61 Å^3, respectively), because all outliers can be explained by a different chemical environment in the reactive region. In the methyl ester groups a strong polarisation is seen with highly positive charges of the contributing carbon atoms (for C9 and C11 > 1.5 e) and accordingly negative charges < −1.0 e for the oxygen atoms O3–O6. For oxirane **2** the atomic charges of C1 and C2 (0.32 and 0.42 e) are greater than for aziridine **1** (0.14 and 0.07 e) and olefin **3** (−0.12 and −0.09 e). This difference is caused by the different electronegativity of O and N. In general, atomic charges are rather poor predictors of reactivity which is confirmed by the present study. Neither the greater reactivity against nucleophiles of the aziridine's C1 *vs.* C2, nor the greater reactivity of the aziridine *vs.* the oxirane can be explained by the atomic charges. As shown in the next sections, the molecules' polarisation patterns induced by intermolecular interactions are much better suited to predict the reactivity.

Intermolecular interactions, lattice and interaction energies

Table 3 shows the hydrogen bond geometries, topological parameters and energies for the three compounds. For aziridine **1**

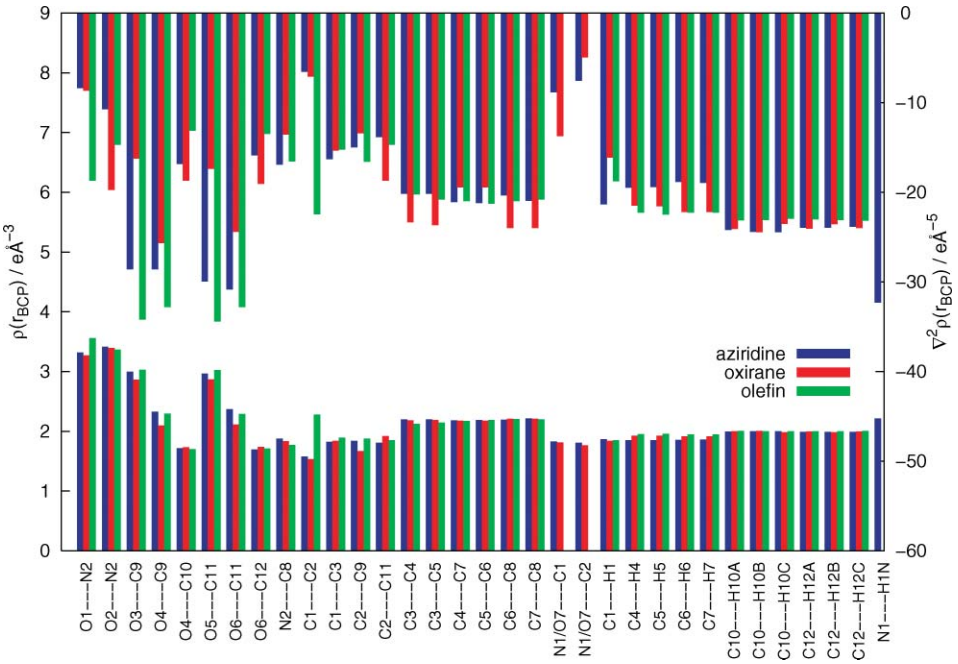

Fig. 4 Electron density (e Å^{-3}) and Laplacian (e Å^{-5}) of the bond critical points of aziridine **1** (average over both datasets and over the two independent molecules of the asymmetric unit), oxirane **2** and olefin **3**.

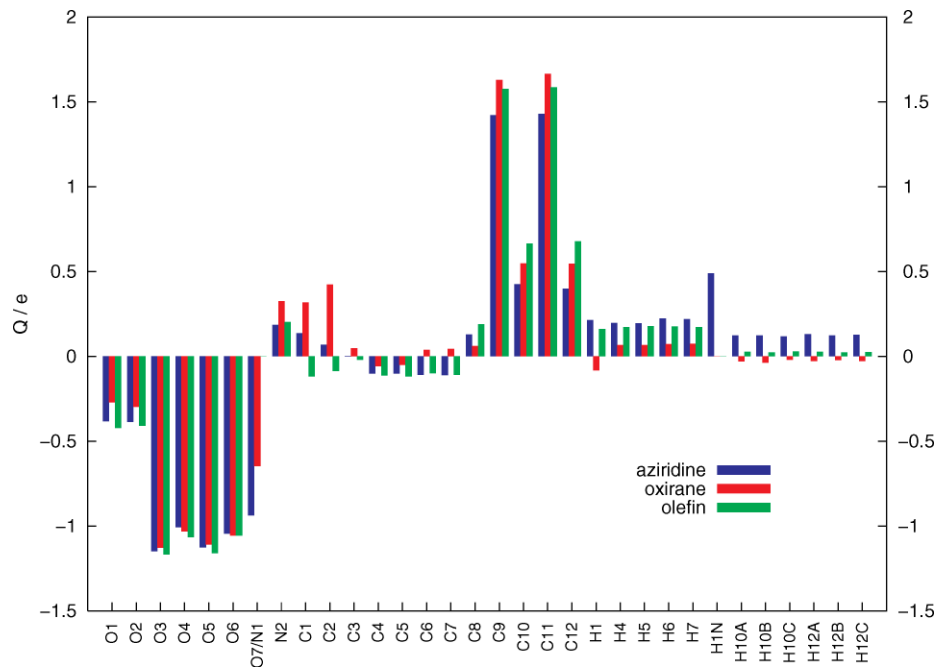

Fig. 5 Atomic charges of compounds **1** to **3**, average over both datasets and over the two independent molecules of the asymmetric unit for aziridine **1**.

average values for the two data sets are shown due to the very small difference in the molecular geometries as mentioned above. Only aziridine **1** exhibits classical hydrogen bonds due to the N–H donor group (a packing diagram of aziridine **1** can be found in ref. 16), but the main stabilising interactions in the crystal are C–H···O/N hydrogen bonds that are not much weaker compared to the classical hydrogen bonds considering the parameters given in Table 3. CH···O/N hydrogen bonds have been found to be very important in several drug binding processes because they stabilise aggregations of molecules with a strength that is suitable for biological processes.[28] Density and Laplacian at the bond critical points correlate with the geometrical parameters of Table 3 in a way Espinosa *et al.* determined,[29] *i.e.* fulfil the exponential Espinosa plots (see Supplementary Material†). The hydrogen bond energies (E_{HB}, see Table 3) calculated after Espinosa *et al.*[30] follow similar correlations. But all these fits of the phenomenological behaviour of experimental data are very inaccurate and well defined correlations as have been established for calculations in the gas phase[31] cannot be found. This is due to the fact that there are many influences between two molecular

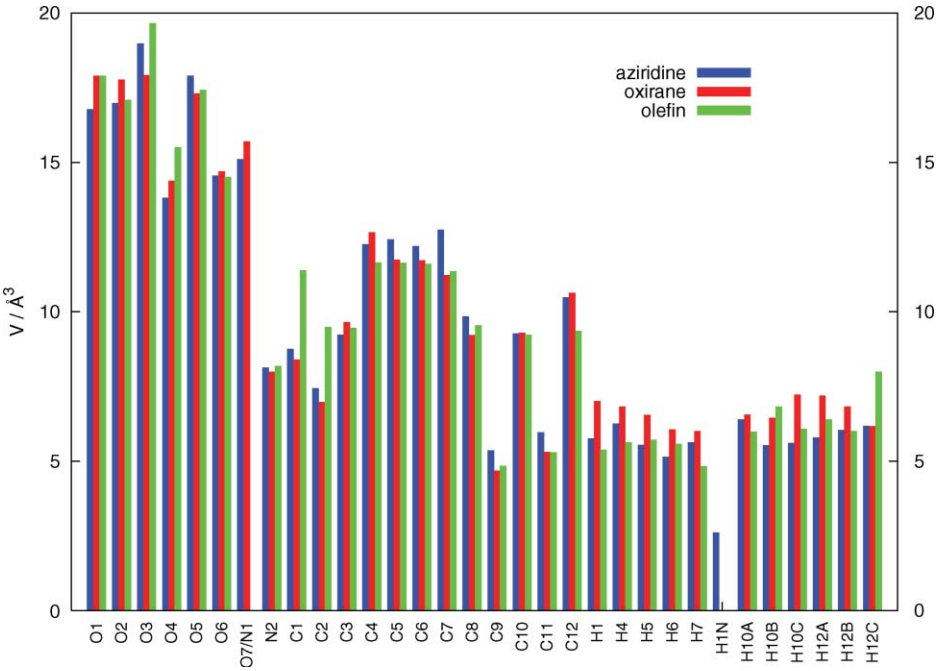

Fig. 6 Atomic volumes of compounds **1** to **3**, average over both datasets and over the two independent molecules of the asymmetric unit for aziridine **1**.

fragments in the crystal that change the parameters of the hydrogen bond between these two fragments significantly. These influences can be taken into account by calculation of the overall interaction energy between these fragments. As it is not possible to extract from the diffraction data the extent to which the density observed is due to intermolecular interactions and how much it is inherent to the molecule itself, it is important to consider energies of the interactions that are accessible and can be calculated within the XDPROP programme of the XD2006 suite[15] in the crystal environment (E_{IA}, see Table 3). The exchange–repulsion terms and the dispersion terms are calculated after Williams and Cox,[32] the electrostatic contribution is calculated after the exact potential/multipole moment hybrid method (EPMM) after Volkov *et al.*[3] The interaction energies between two symmetry related

Table 3 Hydrogen bond geometries, topological parameters and energies, average values for the two data sets of aziridine **1**

Donor-H···acceptor	r(H···acc)/Å	r(don···acc)/Å	a(don-H···acc)/°	ρ/e Å^{-3}	$\nabla^2\rho$/e Å^{-5}	E_{HB}[c]/kJ mol^{-1} a_0^{-3}	E_{IA}[d]/kJ mol^{-1}
Aziridine **1**:							
N(1A)[a]–H(1NA)···O(5A)[e]	2.22	3.12	147	0.09(3)	1.6(1)	−9.54	−12.19
N(1)–H(1 N)···N(1A)[f]	2.22	3.22	170	0.10(4)	1.1(1)	−5.76	−16.13
C(5)–H(5)···O(1)[g]	2.44	3.44	154	0.04(3)	0.7(1)	−4.18	−16.84
C(5A)–H(5A)]···O(1A)[h]	2.45	3.48	158	0.04(3)	0.7(1)	−4.22	−22.82
C(6)–H(6)···O(4)[i]	2.35	3.25	139	0.07(2)	1.1(1)	−6.43	−31.82
C(7)–H(7)···O(5)[h]	2.34	3.15	130	0.07(2)	1.2(1)	−7.18	−16.92
C(7A)–H(7A)···O(5A)[g]	2.46	3.23	126	0.07(2)	1.1(1)	−6.47	−22.83
C(10)–H(10B)···O(6A)	2.43	3.43	157	0.06(1)	0.8(1)	−4.50	−18.31
C(12A)–H(12D)[b]···N(1)[j]	2.39	3.39	155	0.08(1)	1.2(1)	−6.92	−14.67
Oxirane **2**:							
C(5)–H(5)···O(1)[k]	2.45	3.49	160	0.05(3)	0.7(1)	−3.97	−7.57
C(6)–H(6)···O(4)[f]	2.31	3.25	144	0.07(2)	1.2(1)	−7.04	−27.78
C(7)–H(7)···O(5)[l]	2.31	3.15	133	0.07(2)	1.2(1)	−7.06	−7.65
C(10)–H(10C)···O(5)[h]	2.52	3.24	123	0.05(1)	0.9(1)	−5.36	−5.97
C(12)–H(12A)···O(6)[m]	2.53	3.46	146	0.04(1)	0.7(1)	−4.03	−5.21
C(12)–H(12C)···O(5)[n]	2.56	3.46	142	0.04(1)	0.6(1)	−3.40	−4.55
Olefin **3**:							
C(4)–H(4)···O(3)[intra]	2.56	3.46	139	0.08(3)	1.0(1)	−5.54	—
C(5)–H(5)···O(1)[o]	2.52	3.59	169	0.04(3)	0.5(1)	−2.74	−4.73
C(7)–H(7)···O(5)[p]	2.24	3.10	134	0.08(2)	1.4(1)	−8.37	−4.68
C(10)–H(10A)···O(2)[q]	2.39	3.43	166	0.05(1)	0.8(1)	−4.63	−30.77

[a] Labels A refer to the second molecule of the asymmetric unit. [b] Atom H12D belongs to the second molecule of the asymmetric unit. [c] Hydrogen bond energy calculated according to Espinosa *et al.*[30]. [d] Interaction energy between both molecules involved in the hydrogen bond, calculated according to Williams and Cox[32] and Volkov[3]. Symmetry operations:[e] $2-x,1-y,2-z$. [f] $1-x,1-y,1-z$. [g] $-1+x,y,z$. [h] $1+x,y,z$. [i] $2-x,2-y,1-z$. [j] $2-x,1-y,1-z$. [k] $x,-1+y,z$. [l] $x,1+y,z$. [m] $2-x,-y,-z$. [n] $1-x,-y,-z$. [o] $1+x,-1+y,z$. [p] $-1+x,+y,z$. [q] $-1-x,1-y,-z$.

molecules in the crystal that are connected by a hydrogen bond are listed in Table 3. As mentioned above, all interactions between the molecules are accounted for (*e.g.* electrostatic interactions between C and O[16] or π-interactions). Therefore, it is not surprising that there is no correlation between the interaction energy and any of the parameters describing the hydrogen bonds. The interactions within the aziridine crystals are in general much stronger than in the other crystals. For example the interactions between the molecules guided by the hydrogen bonds C7–H7 ··· O5 and C5–H5 ··· O1 that are common to all three compounds are much stronger within the aziridine crystals (about 10 kJ mol^{-1}). This is a meaningful hint for aziridine **1** being more suited for drug design purposes.

The lattice energy of a molecule in the crystal environment can be calculated with XD2006[15] using the same methods as described for the interaction energies. This yields a total crystal binding energy of −161.06 kJ mol^{-1} for oxirane **2** (57% coming from the sum of exchange–repulsion and dispersion and 43% from electrostatic interactions) and −181.87 kJ mol^{-1} for olefin **3** (53.5% from exchange–repulsion and dispersion, 46.5% from electrostatic). For aziridine **1** an average over the two independent molecules of the asymmetric unit was calculated, being −177.70 kJ mol^{-1} for the synchrotron data set (44% exchange–repulsion and dispersion, 56% electrostatic) and −183.24 kJ mol^{-1} for the Mo-K_α data set (43% exchange–repulsion and dispersion, 57% electrostatic). Therefore, the experimental uncertainty is about 6 kJ mol^{-1} so that the values for aziridine **1** and olefin **3** should be considered as equal. As a temperature dependency of the lattice energy is known at least for some inorganic salts,[33] the value for oxirane **2** might not be directly comparable to aziridine **1** and olefin **2** because the data set of oxirane **2** was measured at a higher temperature (100 K instead of 27 or 9 K).

In general, one can state that the lattice energies are quite high for molecular crystals which argues for effective intermolecular binding networks (compare for example crystals of pure benzene that exhibit a much weaker network of intermolecular interactions: lattice energy extrapolated to 0 K = −52.30 kJ mol^{-1};[34] lattice energy calculated with XD2006 for 110 K = −55.50 kJ mol^{-1}, diffraction data taken from ref. 35). Moreover, it is very interesting that the electrostatic contribution for aziridine **1** is greater than 50% whereas it is smaller than 50% for oxirane **2** and olefin **3**. The reason is that only aziridine **1** contains a donor for classical hydrogen bonds and that the C–H ··· X hydrogen bonds are generally stronger in aziridine **1** (see above). So this is another meaningful hint that aziridine **1** is suited better for the described pharmacological purposes because the first ligand-binding step in this biological process is mainly electrostatically controlled. It is in agreement with the fact that aziridine **1** is reactive but oxirane **2** and olefin **3** are not reactive in model reactions regarding a nucleophilic attack (see section on model reactions).

Electrostatic potentials and zero Laplacian isosurfaces

In 1987, Bader stated that "an outer contour of the charge density could be used to assign a size and a shape to a molecule for its nonbonded interactions with other molecules, that is, define the van der Waals envelope".[36] It was shown that the 0.001 au contour yielded a reasonable chemical model for a molecular surface of organic compounds. To correlate the biological activity with the electrostatic potential it has become common practise to scrutinise the electrostatic potential on a molecular surface of 0.001 au (=0.0067 e Å^{-3}).[37] Fig. 7 shows the electrostatic potential of aziridine **1** mapped on the molecular surface at 0.0067 e Å^{-3}. The differently polarised regions that determine how the molecule

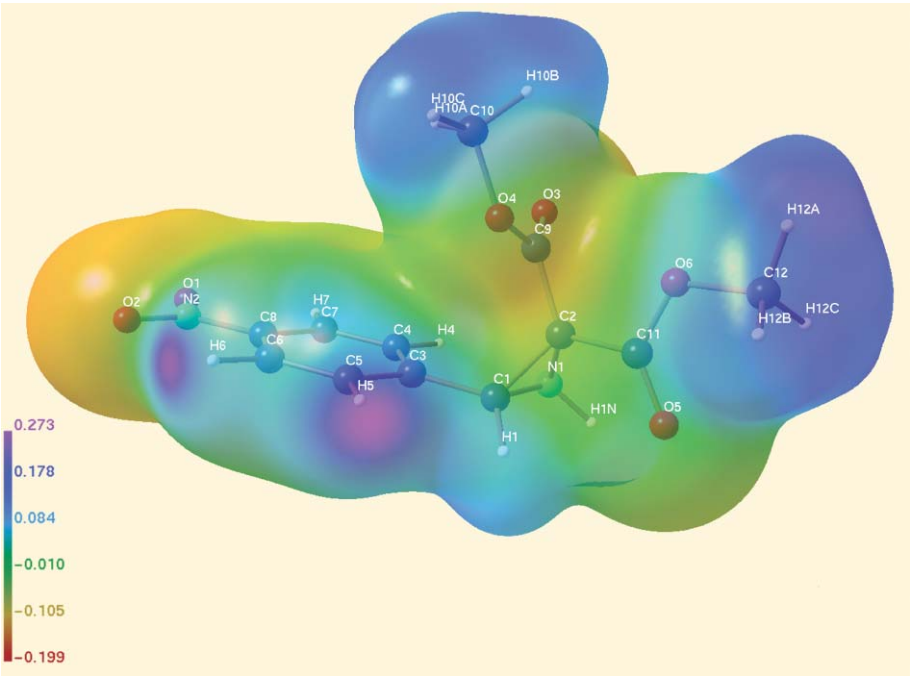

Fig. 7 MOLISO[39] representation: electrostatic potential in e Å^{-1} of aziridine **1**, mapped on an isosurface of the electron density at 0.0067 e Å^{-3} (=0.001 au).

sticks into the enzyme by non-bonding interactions can clearly be distinguished (positive methyl and hydrogen regions, negative nitro region and π-electron cloud of the aryl ring). A difference in the polarisation sphere of the carbon atoms C1 and C2 is observed. Carbon atom C1 is surrounded by a positively polarised region whereas the region around carbon atom C2 is more negatively polarised. The preceding agglomeration of the nucleophilic ring opening reaction could already be guided by this polarisation difference so that C1 shows up as the preferred reaction site. This has also been found by a comparison with theoretically derived data in ref. 16. With respect to the corresponding electrostatic regions on the 0.0067 e Å^{-3} molecular surfaces of oxirane **2** and olefin **3**, no clear distinction between carbon atoms C1 and C2 can be made.

Murray, Politzer *et al.* introduced parameters to quantify the electrostatic potential on the 0.0067 e Å^{-3} molecular surface and relate it to biological reactivity and activity.[37] One of these quantities is the average deviation Π from the mean surface potential that is a measure of the internal charge separation or local polarity which is present even in molecules having zero dipole moment. For compounds **1** to **3** the values of Π are (average over both data sets for aziridine **1**): Π(cpd. **1**) = 0.089 e Å^{-1}, Π(cpd. **2**) = 0.035 e Å^{-1} and Π(cpd. **3**) = 0.079 e Å^{-1}. These differences in the overall polarisation are caused by the different intermolecular interactions and the structural differences in the reactive regions. As discussed in the chapter on intermolecular interactions (see above), the intermolecular bonding network for aziridine **1** is stronger than for the other compounds and is therefore responsible for the greater overall polarisation. Chemical preparative work also shows that aziridine **1** is reactive, the other two compounds are not (see section on model reactions).

To obtain information about the location of possible electrophilic centres that can be target of a nucleophilic attack followed by the forming of a covalent bond, an electrostatic potential mapped on a density surface that is much closer to the nuclei should be examined. Whereas the nuclei have a distance of about 2.0 to 2.5 Å from the 0.0067 e Å^{-3} isosurface (compare: van der Waals − radius of carbon = 1.85 Å), the distance of the nuclei to an 0.5 e Å^{-3} isosurface is about 0.7 to 1.0 Å (compare: covalence radius of carbon = 0.77 Å). The electrostatic potential on this isosurface has been shown in several applications to be a good choice if one wants to examine the impact of individual atoms on the potential without neglecting crystal effects.[16,38] Fig. 8a–c show the electrostatic potential of aziridine **1**, oxirane **2** and olefin **3** on the density isosurface of 0.5 e Å^{-3}. Several maxima (green/blue colour) in the reactive region can be found on the isosurface. Table 4 shows the number, the labelling and the value of the maxima that can be attributed to either carbon atom C1 or C2.

The absolute values of the maxima are not meaningful because they are dependent on the value of the isosurface. The average difference between corresponding maxima on the 0.5 e Å^{-3} isosurface in the two datasets of aziridine **1** is 0.04 e Å^{-1}. Being aware of this uncertainty, one can only state that there is a trend for aziridine **1** and olefin **3** that the values for the maxima at Cl are somewhat larger in contrast to oxirane **2** where the values for the maxima at C2 are somewhat larger. But in all cases the maximum labelled *1a* seems to be the sterically most favorable reaction site (see section on geometric results) because there is no bulky sidechain and no negatively polarised carbonyl oxygen atom nearby as it is in the case of the maxima around C2. All the other maxima at C1 cannot be attacked from the direction of the flat aryl plane but only from the side of the aryl group. The maxima *1a* have the highest value of the maxima around C1 in each case and are about 55 to 75% of the absolute maximum in the compound (also shown in Table 4).

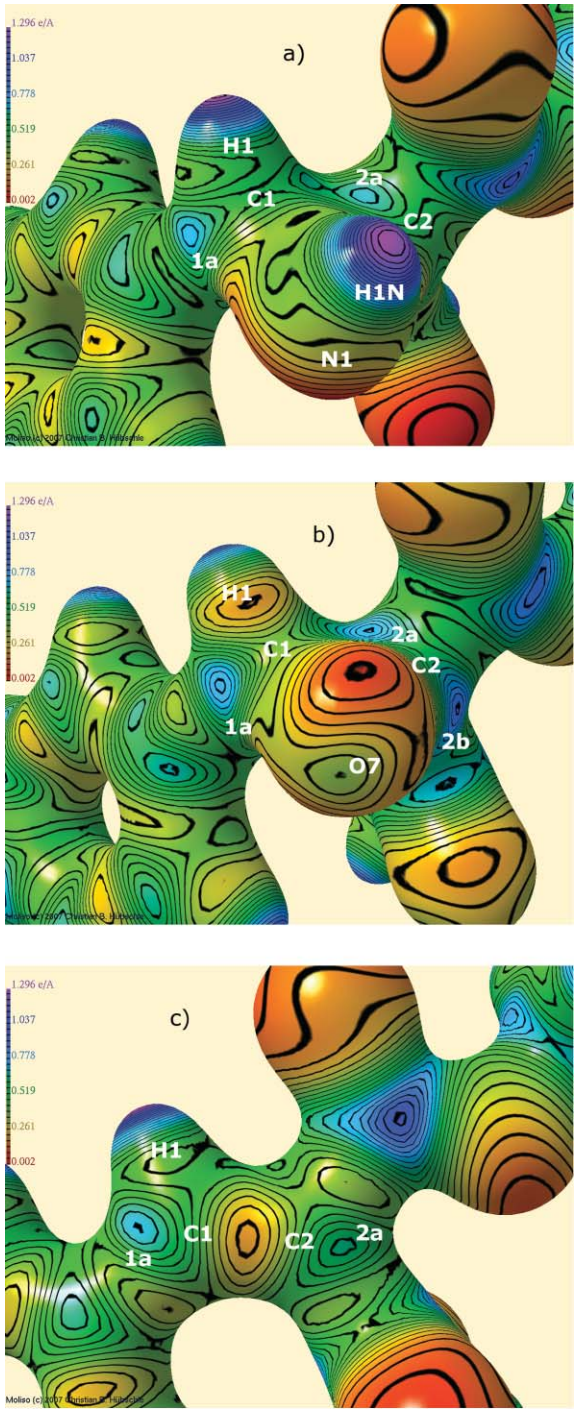

Fig. 8 MOLISO[39] representation: electrostatic potential in e Å^{-1} of the reactive regions of a) aziridine **1**, b) oxirane **2** and c) olefin **3**, mapped on an isosurface of the electron density at 0.5 e Å^{-3}. Positions of atoms under the surface and of maxima of the esp at C1 and C2 are plotted.

Table 4 Maxima of the electrostatic potential (esp) in e Å^{-1} on an isosurface of the electron density at 0.5 e Å^{-3} in the reactive region of cpds. **1** to **3**, see Fig. 8

Label (seen in parts in Fig. 8)	Near atom	Value of esp
Aziridine **1** sync:		
1a	C1	0.73
1b	C1	0.72
1c	C1	0.67
2a	C2	0.68
2b	C2	0.67
	H1N	1.30 (abs. max.)
Aziridine **1** Mo-K$_\alpha$:		
1a	C1	0.73
1b	C1	0.69
1c	C1	0.71
2a	C2	0.63
2b	C2	0.61
	H1N	1.24 (abs. max.)
Oxirane **2**:		
1a	C1	0.79
1b	C1	0.66
1c	C1	0.59
1d	C1	0.57
2a	C2	0.82
2b	C2	0.86
2c	C2	0.77
	H1	1.08 (abs. max.)
Olefin **3**:		
1a	C1	0.70
1b	C1	0.65
2a	C2	0.62
	H1	1.30 (abs. max.)

The zero Laplacian isosurface (defined by $\nabla^2\rho = 0$) shows the location of electrophilic centres by means of reduced valence shell charge concentrations (reduced VSCCs). Therefore, it is called the "reactive surface".[2,40] These reduced VSCCs appear as holes in the surface. Fig. 9 shows the isosurfaces of compounds **1** to **3**. There are larger reduced VSCCs at carbon atom Cl for aziridine **1** (four large holes at C1, two large and one small hole at C2) and larger reduced VSCCs at carbon atom C2 for oxirane **2** (four large holes at C2, two large and two small holes at C1) as there were also found larger values of the esp maxima (see Table 4) at carbon atom C1 for aziridine **1** and at carbon atom C2 for oxirane **2**. Therefore the greater reactivity of aziridine **1** can be explained by the fact that for aziridine **1** carbon atom C1 is both sterically and electronically favoured but for oxirane **2** carbon atom C2 is electronically favoured but sterically hindered. Further important information from the zero Laplacian isosurfaces are the positions of the reduced VSCCs around the atoms. Although the number of the reduced VSCCs and the number of the maxima in the esp do not agree in each case the agreement of their positions is quite high. Especially on the positions where the maxima in the esp labelled *1a* were found there can be found reduced VSCCs in the Figs. 9a–c, too. This is another hint that this sterically most favorable position is also electronically preferred.

Source function

The source function[4] is a relatively new tool to analyse the electron-density distribution. It is calculated directly from the density. The value of the density at any given point can be deconstructed into contributions from all the atomic basins in the molecule. Normally, a bond critical point (bcp) is chosen as reference point

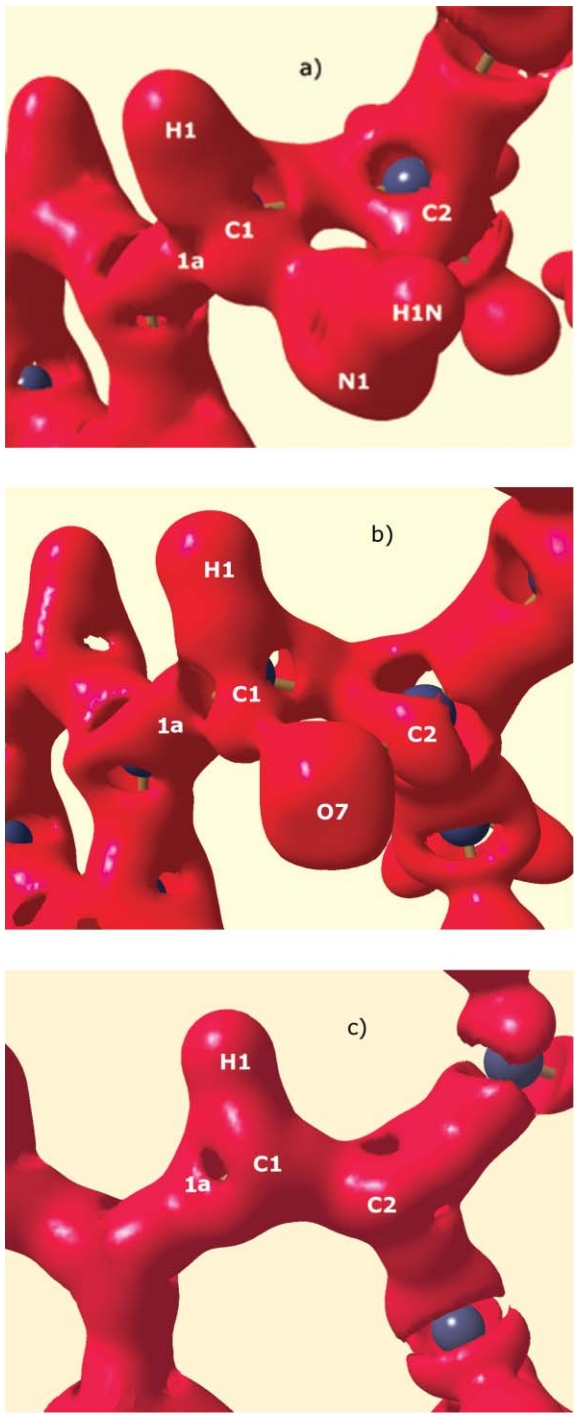

Fig. 9 MOLISO[39] representation: zero Laplacian isosurface of the reactive regions of a) aziridine **1**, b) oxirane **2** and c) olefin **3**.

and the source contributions serve as a measure of the electronic delocalisation regarding this special bond. It can be examined how adjacent atoms or substituents affect the electronic situation of the bond for which the bond critical point is the representative.

Fig. 10 represents the percentage source contributions for the reference points bcp(X–C1) and bcp(X–C2) of aziridine **1** and oxirane **2**, atoms with a source contribution of less than 1% are not shown for clarity. As expected for both cpds. **1** and **2**, the major contributions to the X–C bond critical points of the

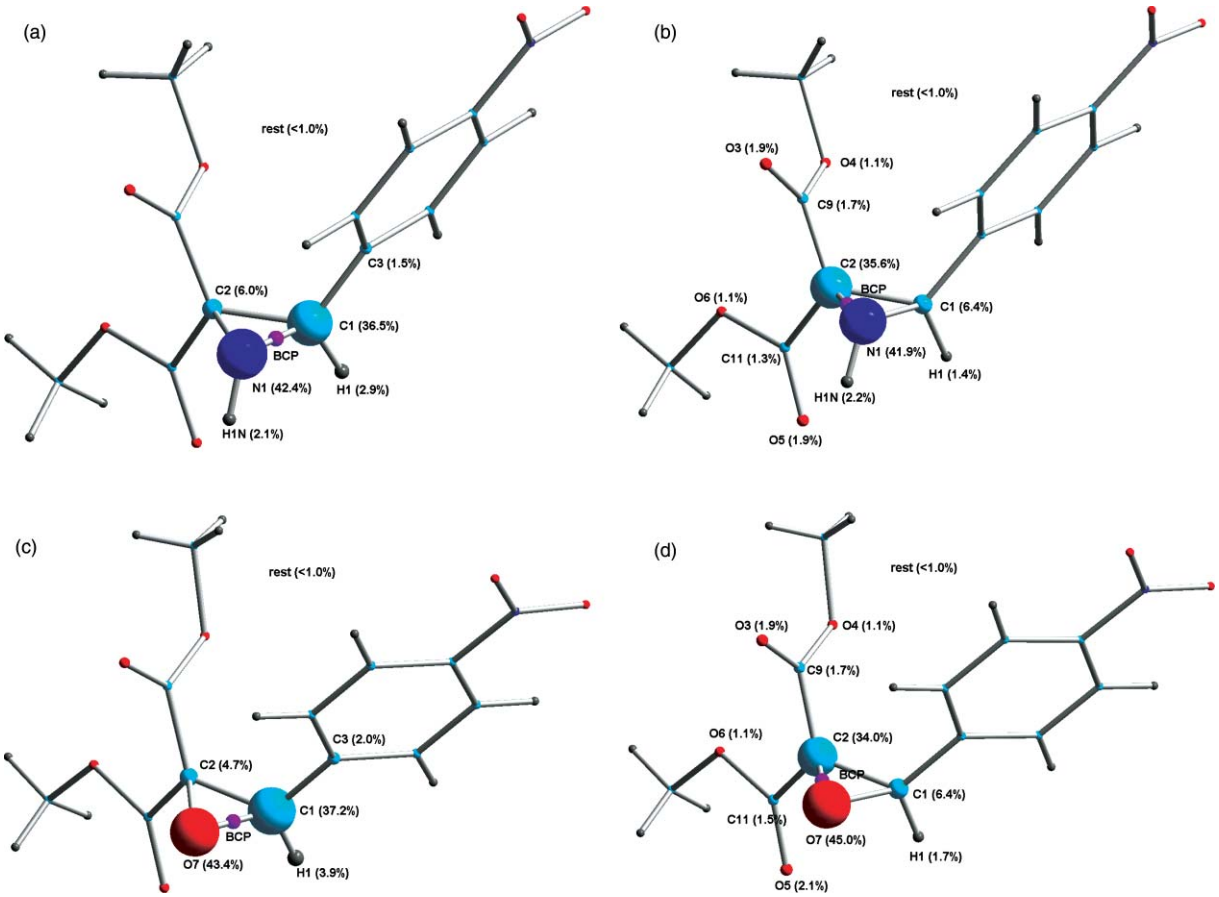

Fig. 10 DIAMOND[41] representation of the percentage source contributions[4] of the atomic basins to the electron density of the N1/O7–C1 bond critical point (left) and the N1/O7–C2 bond critical point (right) of cpds. **1** and **2**.

three-membered rings come from the directly bonded atoms (see Fig. 10). In each case, about 45% of the density comes from the basin of the hetero atom and 35% from the carbon atom. Hence, from the perspective of the source function there seems to be no difference whether the hetero bonds in the three-membered ring are O–C or HN–C bonds.

The minor contributions can be summarised as follows. The contribution of the entire nitrophenyl substituent to the N1–C1 bond is 4.4%, to the O7–C1 bond is 5.5%. Each of the two methoxycarbonyl (MOC) groups contributes with 5.1% to N1–C2 and with 5.5% to O7–C2. It follows that the influence of each of the large substituents to the adjacent X–C bond in the heterocycle is almost the same. If all substituents to C1 (nitrophenyl group plus hydrogen atom) and C2 (two MOC groups) are considered, the influence to the N1/O7–C1 bond adds up to 7/9% and to the N1/O7–C2 bond to 10/11%. The contributions of the substituents to the density of the X–C bond critical points that are not directly bonded to are in each case about 2.5%. In total, the effects of the substituents are by 2–3% larger for the X–C2 than for the X–C1 bonds.

For the bond critical point of C1–C2 the following was found. In the case of olefin **3** 85% of the density comes from the atoms C1 and C2 in equal amounts. But for aziridine **1** and oxirane **2** only 65% comes from these atoms. A significant amount (about 15%) comes from the hetero atom. There is also more interaction with the substituents in the case of compounds **1**/**2** (4.5%/5.3% from the nitrophenyl group and 5.0%/5.7% from each MOC group) compared to olefin **3** (3.4% from the nitrophenyl group and 3.1% from each MOC group). So the electronic situation in the rings is more influenced by the substituents than in case of the double bond. This might be the known effect of activating a double bond by epoxidation or aziridination.

Model reactions with sulfur-, nitrogen- and oxygen nucleophiles

The electrophilic building blocks were subjected to reaction with equimolar amounts of benzyl mercaptane, benzyl amine or acetic acid, respectively, in refluxing toluene-d_8. Samples for NMR spectroscopy and LC-MS were taken after 2, 4, and 8 h.

The NMR- and LC-mass spectra of the reaction of aziridine **1** with benzyl mercaptane as a nucleophile show the dimerisation to the imidazolidine **6** as already published,[42] and the mercaptane adduct **4**[16] (see Scheme 1). The spectra obtained with oxirane **2** or olefin **3** which were treated in the same manner do not show any conversion.

In case of the model reaction with benzyl amine as a nucleophile the benzyl amine adduct **5** (see Scheme 1) could be detected together with the imidazolidines **6**[42] and **7**. Again, no conversion was observed with the oxirane **2** and the olefin **3**.

In case of the reaction with acetic acid no adduct could be observed neither with the aziridine **1**, nor with the oxirane **2** and

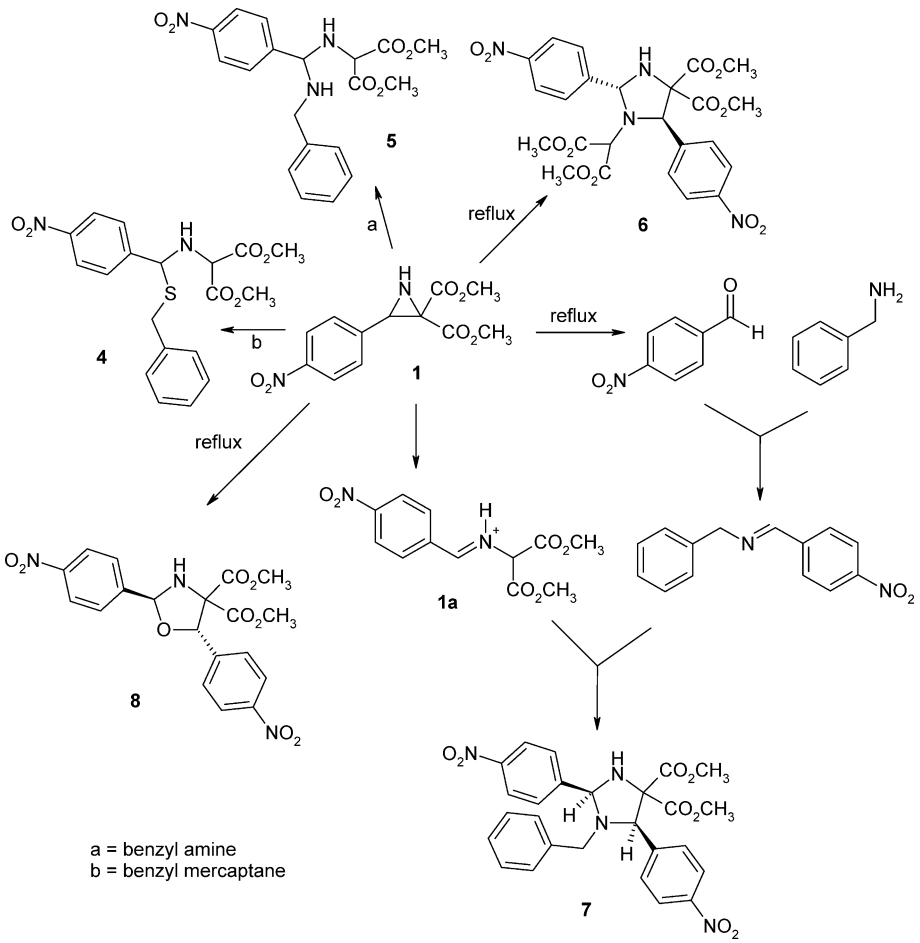

Scheme 1 Reaction pathways of aziridine **1** with benzyl mercaptane or benzyl amine, respectively.

the olefin **3**. Only formation of the already known oxazolidine **8**[42] was observed (Scheme 1).

In summary, only aziridine **1** shows reactivity against the S- or N-nucleophiles. Besides the adducts formed by nucleophilic ring opening after attack at C1 (cpds. **4** and **5**) several products resulting from 1,3-dipolar cycloadditions of **1** could be detected: **6**, by dimerisation of aziridine **1**; **7**, by cycloaddition of **1** with the imine formed by condensation of the decomposition product *p*-nitrobenzaldehyde and benzyl amine; **8**, by cycloaddition of **1** with *p*-nitrobenzaldehyde.

Conclusions

This study shows that the experimental electron-density determination grants access to the structural and electronic properties of biologically active molecules or their model compounds through various tools that can directly be derived from the density. Therefore, these tools can be exploited for the development, optimisation and analysis of pharmaceutically relevant compounds. Screenings over promising compounds can be carried out at synchrotron beamlines where the exposure time periods for one measurement are in the range of a few hours at present but should decrease at new synchrotron sources with much higher primary intensity. One aspect of this work was to show in which range the reproducibility and therewith the error of two measurements under different experimental conditions (in-house *vs.* synchrotron) lies. It has been found for several parameters like geometry, topological and atomic properties or electrostatic potential that the reproducibility is quite good and comparable to other studies. Comparing the topological parameters between the different compounds, transferability within the error margins of reproducibility that is a crucial property in a Bader analysis could be found.

Three protease inhibitor model compounds—aziridine **1**, oxirane **2** and olefin **3**—have been examined regarding their biological activity and general reactivity. Aziridine **1** is most suitable for drug design. It is most reactive because it is outstanding in the properties that can be related to the reactivity of the intermolecular hydrogen-bonding network, the lattice and interaction energies and the electrostatic potential. The regioselectivity of the reaction (nucleophilic attack at carbon atom C1 rather than at carbon atom C2) for aziridine **1** was found within steric considerations, and the electrostatic potential. Moreover, hints for the stereoselectivity, that means the preferred reaction site at carbon atom C1, could be found by examining the electrostatic potential at a molecular surface of 0.5 e $Å^{-3}$ and the zero Laplacian isosurfaces. The source function showed the influence of the two different substituents (nitrophenyl and methoxycarbonyl group) on the density of the bond critical points in the reactive region.

In general, the intermolecular interaction network that influences several properties like interaction energies and electrostatic

potentials is crucial for the activity (reactivity plus selectivity) of the compound, the electronegativity difference between O and N is not decisive. These findings were proven by preparative model reactions: aziridine **1** is reactive and the reaction is specific at C1, oxirane **2** and olefin **3** are not reactive.

We believe that the recent methodical developments elaborated in this work open up a spectrum of tools that can be exploited in the future for drug development purposes.

Acknowledgement

This investigation was supported by grants of the DFG within SPP 1178.

References

1 (*a*) G. Naray-Szabo, *J. Mol. Graphics*, 1989, **7**, 76–81; (*b*) G. Naray-Szabo, *J. Mol. Graphics*, 1989, **7**, 98.
2 R. F. W. Bader, *Atoms in Molecules – A Quantum Theory*, Clarendon Press, Oxford, 1995.
3 A. Volkov, T. Koritsánszky and P. Coppens, *Chem. Phys. Lett.*, 2004, **391**, 170–175.
4 (*a*) R. F. W. Bader and C. Gatti, *Chem. Phys. Lett.*, 1998, **287**, 233–238; (*b*) C. Gatti, F. Cargnoni and L. Bertini, *J. Comput. Chem.*, 2003, **24**, 422–436; (*c*) C. Gatti and L. Bertini, *Acta Crystallogr., Sect. A*, 2004, **60**, 438–449; (*d*) J. Overgaard, B. Schiøtt, F. K. Larsen and B. B. Iversen, *Chem.–Eur. J.*, 2001, **7**, 3756–3767.
5 (*a*) J. C. Powers, J. L. Asgian, O. D. Ekici and K. E. James, *Chem. Rev.*, 2002, **102**, 4639–4750; (*b*) H.-H. Otto and T. Schirmeister, *Chem. Rev.*, 1997, **97**, 133–171.
6 (*a*) B. M. Dunn, *Chem. Rev.*, 2002, **102**, 4431–4458; (*b*) B. Degel, P. Staib, S. Rohrer, J. Schreiber, E. Martina, C. Büchold, K. Baumann, J. Morschhäuser and T. Schirmeister, *ChemMedChem*, 2008, **3**, 302–315.
7 (*a*) R. Vikic, M. Busemann, C. Gelhaus, N. Stiefl, W. Schmitz, F. Schulz, M. Mladenovic, B. Engels, M. Leippe, K. Baumann and T. Schirmeister, *ChemMedChem*, 2006, **1**, 1126–1141; (*b*) R. Vikic, H. Helten, T. Schirmeister and B. Engels, *ChemMedChem*, 2006, **1**, 1021–1028; (*c*) T. Schirmeister and A. Klockow, *Mini-Rev. Med. Chem.*, 2003, **3**, 585–596.
8 (*a*) R. Vikic, M. Busemann, K. Baumann and T. Schirmeister, *Curr. Top. Med. Chem.*, 2006, **6**, 331–353; (*b*) M. S. Lall, R. P. Jain and J. C. Vederas, *Curr. Top. Med. Chem.*, 2004, **4**, 1239–1253.
9 (*a*) E. Martina, N. Stiefl, B. Degel, F. Schulz, A. Breuning, M. Schiller, R. Vikic, K. Baumann, J. Ziebuhr and T. Schirmeister, *Bioorg. Med. Chem. Lett.*, 2005, **15**, 5365–5369; (*b*) S. H. L. Verhelst and M. Bogyo, *ChemBioChem*, 2005, **6**, 824–827; (*c*) S. Ro, S. G. Baeck, B. Lee and J. H. Ok, *J. Pept. Res.*, 1999, **54**, 242–248.
10 U. Kaeppler, N. Stiefl, M. Schiller, R. Vikic, A. Breuning, W. Schmitz, D. Rupprecht, C. Schmuck, K. Baumann, J. Ziebuhr and T. Schirmeister, *J. Med. Chem.*, 2005, **48**, 6832–6842.
11 (*a*) P. Luger, *Org. Biomol. Chem.*, 2007, **5**, 2529–2540; (*b*) P. Luger, A. Wagner, C. B. Hübschle and S. I. Troyanov, *J. Phys. Chem. A*, 2005, **109**, 10177–10179 .
12 *Bruker-AXS inc., SAINT*, 1994–1996, Madison, WI, USA.
13 W. Kabsch, *XDS* (version 08/2006) in: (*a*) W. Kabsch, *J. Appl. Crystallogr.*, 1988, **21**, 916–924; (*b*) W. Kabsch, *J. Appl. Crystallogr.*, 1993, **26**, 795–800.
14 S. K. J. Johnas and E. Weckert, *A Program for Oblique Incidence Correction* in: S. K. J. Johnas, W. Morgenroth and E. Weckert, *HASYLAB Annual Report*, 2006, 325–328.
15 A. Volkov, P. Macchi, L. J. Farrugia, C. Gatti, P. Mallinson, T. Richter, and T. Koritsánszky, *XD2006 – A Computer Program for Multipole Refinement, Topological Analysis of Charge Densities and Evaluation of Intermolecular Energies from Experimental or Theoretical Structure Factors*, version 5.34, 2006.
16 S. Grabowsky, T. Pfeuffer, L. Chęcinska, M. Weber, W. Morgenroth, P. Luger and T. Schirmeister, *Eur. J. Org. Chem.*, 2007, **17**, 2759–2768.
17 R. H. Blessing, *SORTAV* in: (*a*) R. H. Blessing and D. A. Langs, *J. Appl. Crystallogr.*, 1987, **20**, 427–428; (*b*) R. H. Blessing, *J. Appl. Crystallogr.*, 1989, **22**, 396–397; (*c*) R. H. Blessing, *J. Appl. Crystallogr.*, 1997, **30**, 421–426.
18 G. M. Sheldrick, *SHELX* in :G. M. Sheldrick, *Acta Crystallogr., Sect. A*, 2008, **64**, 112–122.
19 N. K. Hansen and P. Coppens, *Acta Crystallogr., Sect. A*, 1978, **34**, 909–921.
20 F. H. Allen, O. Kennard, D. G. Watson, L. Brammer, A. G. Orpen and R. Taylor, in *International Tables for Crystallography, Volume C*, ed. A. J. C. Wilson, Kluwer Academic Publishers, Dordrecht, Boston, London, 1992, ch. 9.5, pp. 685–706.
21 C. B. Hübschle and B. Dittrich, *INVARIOMTOOL* in: C. B. Hübschle, P. Luger and B. Dittrich, *J. Appl. Crystallogr.*, 2007, **40**, 623–627.
22 (*a*) B. Dittrich, C. B. Hübschle, P. Luger and M. Spackman, *Acta Crystallogr., Sect. D*, 2006, **62**, 1325–1335; (*b*) B. Dittrich, T. Koritsánszky and P. Luger, *Angew. Chem.*, 2004, **116**, 2773–2776; B. Dittrich, T. Koritsánszky and P. Luger, *Angew. Chem., Int. Ed.*, 2004, **43**, 2718–2721.
23 E. Keller, *SCHAKAL-99, A Fortran Program for the Graphical Representation of Molecular and Solid-State Structure Models* in: E. Keller, *Chem. Unserer Zeit*, 1980, **14**, 56-60.
24 P. Luger, C. Zaki, J. Buschmann and R. Rudert, *Angew. Chem.*, 1986, **98**, 254–255; P. Luger, C. Zaki, J. Buschmann and R. Rudert, *Angew. Chem., Int. Ed. Engl.*, 1986, **25**, 276–277.
25 (*a*) A. Volkov and P. Coppens, *Acta Crystallogr., Sect. A*, 2001, **57**, 395–405; (*b*) J. Henn, D. Ilge, D. Leusser, D. Stalke and B. Engels, *J. Phys. Chem. A*, 2004, **108**, 9442–9452.
26 L. Chęcinska, S. Mebs, C. B. Hübschle, D. Förster, W. Morgenroth and P. Luger, *Org. Biomol. Chem.*, 2006, **4**, 3242–3251.
27 B. Dittrich, T. Koritsánszky, M. Grosche, W. Scherer, R. Flaig, A. Wagner, H. G. Krane, H. Kessler, C. Riemer, A. M. M. Schreurs and P. Luger, *Acta Crystallogr., Sect. B*, 2002, **58**, 721–727.
28 (*a*) J. Sola, A. Riera, X. Verdaguer and M. A. Maestro, *J. Am. Chem. Soc.*, 2005, **127**, 13629–13633; (*b*) J. P. Glusker, *Acta Crystallogr., Sect. D*, 1995, **51**, 418–427; (*c*) P. M. Takahara, C. A. Frederick and S. J. Lippard, *J. Am. Chem. Soc.*, 1996, **118**, 12309–12321.
29 E. Espinosa, M. Souhassou, H. Lachekar and C. Lecomte, *Acta Crystallogr., Sect. B*, 1999, **55**, 563–572.
30 E. Espinosa, E. Molins and C. Lecomte, *Chem. Phys. Lett.*, 1998, **285**, 170–173.
31 (*a*) J. Beckmann and S. Grabowsky, *J. Phys. Chem. A*, 2007, **111**, 2011–2019; (*b*) S. J. Grabowski, *Chem. Phys. Lett.*, 2001, **338**, 361–366; (*c*) M. Ziolkowski, S. J. Grabowski and J. Leszczynski, *J. Phys. Chem.*, 2006, **110**, 6514–6521.
32 D. E. Williams and S. R. Cox, *Acta Crystallogr., Sect. B*, 1984, **40**, 404–417.
33 M. Subrahmanyam, E. Rajagopal and N. Manohara Murthy, *Indian J. Pure Appl. Phys.*, 2005, **43**, 660–663.
34 D. J. Evans and R. O. Watts, *Mol. Phys.*, 1976, **31**, 83–96.
35 H.-B. Bürgi, S. C. Capelli, A. E. Goeta, J. A. K. Howard, M. A. Spackman and D. S. Yufit, *Chem.–Eur. J.*, 2002, **8**, 3512–3521.
36 R. F. W. Bader, M. T. Carroll, J. R. Cheeseman and C. Chang, *J. Am. Chem. Soc.*, 1987, **109**, 7968–7979.
37 (*a*) J. S. Murray, P. Lane and P. Politzer, *J. Am. Chem. Soc.*, 1995, **85**, 1–8; (*b*) P. Politzer, J. S. Murray and Z. Peralta-Inga, *Int. J. Quantum Chem.*, 2001, **85**, 676–684.
38 (*a*) C. B. Hübschle, S. Scheins, M. Weber, P. Luger, A. Wagner, T. Koritsánszky, S. I. Troyanov, O. V. Boltalina and I. V. Goldt, *Chem.–Eur. J.*, 2007, **13**, 1910–1920; (*b*) D. Förster, S. Scheins, P. Luger, D. Lentz and W. Preetz, *Eur. J. Inorg. Chem.*, 2007, **20**, 3169–3171.
39 C. B. Hübschle, *MolIso* in: C. B. Hübschle and P. Luger, *J. Appl. Crystallogr.*, 2006, **39**, 901–904.
40 W. Chan and I. P. Hamilton, *J. Chem. Phys.*, 1998, **108**, 2473–2485.
41 G. Bergerhoff, M. Berndt and K. Brandenburg, *DIAMOND* in: G. Bergerhoff, M. Berndt and K. Brandenburg, *J. Res. Natl. Inst. Stand. Technol.*, 1996, **101**, 221–225.
42 T. Schirmeister, *Liebigs Ann.*, 1997, 1895–1899.